Co(II) macrocyclic complexes appended with fluorophores as paraCEST and cellCEST agents

Akanksha Patel¹, Samira M. Abozeid¹, Paul J. Cullen² and Janet R. Morrow^{1*}

- Department of Chemistry, University at Buffalo, the State University of New York, Amherst, NY 14260
- 2. Department of Biological Sciences, University at Buffalo, the State University of New York, Amherst, NY 14260

Abstract

Four high spin macrocyclic Co(II) complexes with hydroxypropyl or amide pendants and appended coumarin or carbostyril fluorophores were prepared as CEST (chemical exchange saturation transfer) MRI probes. The complexes were studied in solution as paramagnetic CEST (paraCEST) agents and after loading into *Saccharomyces cerevisiae* yeast cells as cell-based CEST (cellCEST) agents. The fluorophores attached to the complexes through an amide linkage imparted an unusual pH dependence to the paraCEST properties of all four complexes through of ionization of a group that was attributed to the amide NH linker. The furthest shifted CEST peak for the hydroxypropyl-based complexes changed by approximately 90 ppm upon increasing the pH from 5 to 7.5. At acidic pH, the Co(II) complexes exhibited three to four CEST peaks with the most highly shifted CEST peak at 200 ppm. The complexes demonstrated substantial paramagnetic water proton shifts which is a requirement for the development of cellCEST agents. The large shift in the proton resonance was attributed to an inner-sphere water at neutral pH, as shown by variable temperature ¹⁷O NMR spectroscopy studies. Labeling of yeast with one of these paraCEST agents was optimized with fluorescence microscopy and validated by using ICP-Mass spectrometry quantitation of cobalt. A weak asymmetry in the Z-spectra was observed in the yeast labeled with Co(II) complex,

towards a cellCEST effect, although the Co(II) complexes were toxic to the cells at the concentrations necessary for observation of cellCEST.

Introduction

The development of transition metal complexes as MRI contrast agents takes advantage of the multiple spin and oxidation states, biological relevance and richly variable coordination chemistry of the first-row d-block elements. Transition metal ions such as Fe(II)/Fe(III), Co(II), or Ni(II) form coordination complexes that serve as alternatives for the more extensively studied lanthanide(III) paraCEST (paramagnetic chemical exchange saturation transfer) agents. ParaCEST agents are members of a class of MRI probe that produce a change in the water proton signal intensity though chemical exchange saturation transfer (CEST). CEST agents contain one or more exchangeable protons that exchange sufficiently slowly to produce distinct resonances for the CEST agent and bulk water on the NMR timescale. The exchangeable protons can be selectively saturated by using a radiofrequency pulse to give a magnetically saturated proton that exchanges with bulk water protons. Z-spectra or CEST spectra show a plot of the percent decrease in the bulk water magnetization as a function of the presaturation radiofrequency pulse.¹⁻⁴

The paramagnetic metal ion in a paraCEST agent serves to shift the exchangeable proton resonance away from that of bulk water though paramagnetic (hyperfine) interactions. ParaCEST agents typically have ligands with exchangeable OH or NH groups that are in close proximity to the paramagnetic center. ParaCEST agents with multiple exchangeable protons that are magnetically inequivalent, either on a single agent or multiple agents, may show distinct CEST peaks that can be simultaneously detected in a single experiment. For example, responsive paraCEST agents are of interest for registering changes in the biological environment. For example, responsive paraCEST agents may demonstrate a dependence of the CEST effect on factors such as temperature, 7,8 pH, 9 or redox potential 5, 10, 11 to detect changes in biological

micro-environment that may be linked to disease states. Responsive agents that have multiple CEST peaks may be used as ratiometric sensors by tracking the relative change of intensity of each peak.

A major disadvantage of CEST and paraCEST agents is that their poor sensitivity necessitates milimolar concentrations of exchangeable protons for detection.⁵ There are many ways to enhance the sensitivity of these CEST agents, and most of them involve loading paramagnetic complexes into supramolecular assemblies.¹²⁻¹⁷ LipoCEST (liposomal CEST) is one of the successful approaches to enhance sensitivity. In this approach, a paramagnetic complex is entrapped into a liposome which leads to a shift in the proton resonance of the large inner pool of liposomal water. Irradiation of these protons with a radiofrequency pulse, followed by exchange through the liposomal bilayer with bulk water leads to a CEST effect.^{5, 18-20} The approach of encapsulation of paramagnetic complexes for shifting of internal water proton resonances can be extended to cells given the permeability of cell membranes to water molecules.^{9, 21, 22} Such labels are utilized to evaluate cell therapy treatments. For example, cell-based CEST (cellCEST) may be used to visualize the localization and repair of cells after an *in vivo* transplant.²³

Our group is focused on developing transition metal complexes as environmentally responsive probes for MRI²⁴⁻²⁹ and also supramolecular approaches for CEST agents.^{30, 31} Towards this goal, we recently reported strong outer-sphere and inner-sphere water interactions in Co(II) complexes with alcohol or amide donors, providing significant paramagnetic shifts to bulk water.³²⁻³⁴ Complexes that strongly paramagnetically shift the ¹H resonances of water are requisite for producing shifted water resonances in the interior of liposomes³⁴ or cells to generate a CEST effect.

In this study, we present four Co(II) complexes with a 1,4,7-triazacyclononane macrocyclic framework (Scheme 1). Three complexes contain hydroxypropyl pendants and an amide pendant with an attached fluorophore, and one complex contains two amide pendants in lieu of the hydroxypropyl pendants. The hydroxyl donors produce strong second-sphere water interactions through extensive hydrogen bonding and the fluorophore enables tracking of the cellular loading of the complexes. These

complexes display multiple highly shifted pH dependent CEST peaks. An unusual feature of these complexes is the large change in CEST peak position from pH 6 to pH 8, corresponding to deprotonation of ligand donors. The presence of an inner-sphere water molecule in all Co(II) complexes at neutral pH is promising for the producing large changes in the bulk water ¹H resonances. Labeling *of Saccharomyces cerevisiae* (Baker's yeast) with Co(II) complexes was studied towards the development of an imaging method to track infections by related fungal species that cause virulence in animals, such as *Candida albicans*. Such cell tracking methods would involve labeling the yeast cells with Co(II) complex and monitoring the labeled yeast in animals through CEST imaging. Fluorescence microscopy of the bimodal Co(II) probes was used to study cellular association and organellar compartmentalization that would have an effect on the exchange of water and protons as an important component of the CEST signal.

Experimental

Instrumentation. A Varian Inova 500 MHz NMR spectrometer equipped with FTS Systems TC-84 Kinetics Air Jet Temperature Controller was used to collect CEST NMR data and ¹H NMR spectra. ¹³C NMR

spectra were acquired using a Varian Mercury 300 MHz NMR spectrometer operating at 75 MHz. ¹⁷O NMR spectra were recorded on a Varian Inova 400 MHz spectrometer equipped with a 5mm broad-band probe operating at a resonance frequency of 54.24 MHz. All pH measurements were obtained by using an Orion 8115BNUWP Ross Ultra Semi Micro pH electrode connected to a 702 SM Titrino pH. ThermoFinnigan LCQ Advantage IonTrap LC/MS equipped with a Surveyor HPLC system was used to collect mass spectral data. Absorbance spectra were collected using Beckman-Coulter DU 800 UV-vis Spectrophotometer equipped with a Peltier Temperature Controller. Fluorescent studies were performed on Cary Eclipse Varian Fluorimeter with a Varian Temperature regulator. Fluorescence microscopy was performed using Zeiss Axioplan2 microscope.

Materials. All solvents and reagents were reagent grade, and they were used as received without additional purification. 7-amino-4-methyl-2-quinolone was obtained from Astatech chemicals. 1,4,7-triazacyclononane (TACN) and S(-)-propylene oxide were purchased from TCI America. Cobalt(II) nitrate and N,N-Diisopropylethylamine was purchased from Alfa Aesar. 2-Bromoacetamide was purchased from ACROS organics. Milli-Q purified water was used to make aqueous solutions. Deuterated solvents were purchased from Cambridge isotope laboratories. Milli-Q purified water was used to make aqueous solutions. Sodium sulfate and buffer 4-(2-hydroxyethyl)-1-piperanineethanesulfonic acid (HEPES) were purchased from Fisher Chemicals. Nitric acid 65-70% ≥99.999% (trace metals basis) was obtained from BeanTown Chemical. 100 ppm Co standard solutions were purchased from Inorganic Ventures.

Synthesis of macrocyclic ligands and complexes

The macrocyclic ligands 2-(4,7-bis((S)-2-hydroxypropyl)-1,4,7-triazonan-1-yl)-N-(4-methyl-2-oxo-1,2-dihydroquinolin-7-yl)acetamide (TOCs) and 2-(4,7-bis((S)-2-hydroxypropyl)-1,4,7-triazonan-1-yl)-N-(2-oxo-4-(trifluoromethyl)-2H-chromen-7-yl)acetamide (TOCO151) were prepared as reported in the literature.²⁷

N-(4-methyl-2-oxo-1,2-dihydroquinolin-7-yl)-2-(1,4,7-triazonan-1-yl)acetamide (TACN-Cs). was synthesized as reported in the literature.²⁷

2,2'-(7-(2-((4-methyl-2-oxo-1,2-dihydroquinolin-7-yl)amino)-2-oxoethyl)-1,4,7-triazonane-1,4-diyl)diacetamide (TACs). TACN-Cs (103. mg, 0.300 mmol) was dissolved in 2 mL EtOH. N,N-Diisopropylethylamine (100 μL, 0.600 mmol) was added to the solution. Excess 2-Bromoacetamide (125 mg, 0.900 mmol) was dissolved in 2 mL of chloroform and added to the reaction mixture. The reaction mixture was stirred 16 h at room temperature. The product was precipitated by the addition of diethyl ether. The precipitate was washed with diethyl ether three times to obtain the product in 63% yield as white solid. 1 H NMR (500 MHz, CD₃OD) δ 7.90 (1H, s), 7.72 (1H, d, J = 8 Hz), 7.45 (1H, d, J = 8 Hz), 6.40 (1H, s), 3.73 (6H, br s), 3.15-2.96 (12H, m), 2.48 (3H, s). 13 C NMR (75 MHz, CD₃OD) δ 171.47 (2C, s), 169.34 (1C, s), 163.97 (1C, s), 149.94 (1C, s), 140.48 (1C, s), 138.62 (1C, s), 125.03 (1C, s), 117.78 (1C, s), 116.79 (1C, s), 115.05 (1C, s), 105.57 (1C, s), 59.1 (1C, s), 56.52 (2C, s), 50.36 (2C, s), 49.54 (2C, s), 48.81 (2C, s), 17.59 (1C, s). ESI-MS of [TACs+H]⁺ calculated: 458.3, found: 459.

[Co(TACs-H⁺)](NO₃). To 10 mL acetonitrile solution of TACs ligand (86.0 mg, 1.88 mmol) was added 5.0 mL acetonitrile solution of $Co(NO_3)_2$ (66.0 mg, 2.25 mmol). After 1 h stirring, the volume of these solutions reduced until 5 ml followed by slow addition of 15 mL of diethyl ether until the complexes precipitated. The complexes were filtered and washed with diethyl ether (10 mL x 3). [Co(TACS-H⁺)](NO₃) was collected as pink solids with yields of 77%. FT-ICR-MS of [Co(TACs-H⁺)-NO₃]⁺calculated: 515.16857; found: 515.16976. Purity % by ICPMS = (measured concentration /calculated concentration) x 100 = 99.86%. Co content through ICP-MS calculated for [Co(TACs-H⁺)NO₃]⁺: 10.19%, found: 10.17 % \pm 0.31 %.

N-(2-oxo-4-methyl-2H-chromen-7-yl)-2-(1,4,7-triazonan-1-yl)acetamide (TACN-Cou121). To a solution of 1,4,7-triazacyclononane (TACN; 800. mg, 6.20 mmol) in acetonitrile was added compound (1) (517 mg, 2.06 mmol) dissolved in acetonitrile. The reaction mixture was stirred at room temperature for

10 minutes, and then the solvent was removed under vacuum. The product was extracted with CHCl₃ and washed with 1 M NaOH, water and saturated brine. The organic layer was dried over Na₂SO₄ and the solvent was removed under vacuum. The product was obtained in 34% yield. 1 H NMR (500 MHz, CD₃OD) δ 7.86 (1H, s), 7.71 (1H, d, 10 Hz), 7.42 (1H, d, 10 Hz), 6.31 (1H, s), 3.33 (2H, s), 2.90 (6H, br, s), 2.80 (6H, br, s), 2.45 (3H, s). 13 C NMR (75 MHz, CD₃OD) δ 172.6 (1C, s), 160.8 (1C, s), 155.1 (2C, s), 143.3 (1C, s), 124.3 (1C, s), 118.6 (1C, s), 112.8 (2C, s), 106.9 (2C, s), 75.5 (1C, s), 49.5 (2C, s), 49.0 (4C, s), 19.4 (1C, s). ESI-MS of [TACN-Cou121+H]⁺ calculated: 355.1, found: 355.

2-(4,7-bis((S)-2-hydroxypropyl)-1,4,7-triazonan-1-yl)-N-(2-oxo-4-methyl-2H-chromen-7-

yl)acetamide (TOCO121). TACN-Cou121 (100. mg, 0.230 mmol) was dissolved in EtOH. Excess (S)-propylene oxide (41 mg, 0.69 mmol) was added to the reaction mixture and was stirred 16 h at room temperature. The solvent and excess (S)-propylene oxide was removed under reduced pressure to obtain the product in 84% yield as yellow oil. 1 H NMR (500 MHz, CD₃OD) δ 7.83 (1H, s), 7.71 (1H, d, J = 10 Hz), 7.50 (1H, d, J = 5Hz), 6.23 (1H, s), 3.91 (2H, br s), 3.63-3.60 (2H, q, 2Hz), 3.32 (2H, s), 2.95-2.90 (6H, m), 2.76-2.66 (6H, m), 2.40 (3H, s), 1.20-1.18 (3H, m), 1.11-1.10 (3H, m). 13 C NMR (101 MHz, CDCl₃) δ 172.6 (1C, s), 160.5 (1C, s), 155.5 (1C, s), 142.1 (1C, s), 124.8 (1C, s), 118.8 (1C, s), 119.0 (1C, s), 116.7 (1C, s), 112.9 (1C, s), 110.0 (1C, s), 65.26 (2C, s), 63.86 (2C, s), 53.82 - 52.27 (6C, m), 20.08 (2C, s), 18.85 (1C, s). ESI-MS of [TOCS+H]⁺ calculated: 460.3, found: 461.

[Co(TOCs-H⁺)](NO₃). To 10 mL ethanolic solution of TOCs ligand (40 mg, 0.087 mmol) was added 5.0 mL ethanolic solution of Co(NO₃)₂ (27 mg, 0.090 mmol). After 1 h stirring, the volume of these solutions reduced until 5 ml followed by slow addition of 15 mL of diethyl ether until the complexes precipitated. The complexes were filtered and washed with diethyl ether (10 mL x 3). [Co(TOCs)](NO₃) was collected as pink solids with yields of 87%. FT-ICR-MS of [Co(TOCs-H⁺)-NO₃]⁺ calculated: 517.217200, found: 517.21016. Purity % by ICPMS = 99.86%. Co content through ICP-MS calculated for [Co(TOCs-H⁺)-NO₃]⁺: 10.19%, found: 10.17 % \pm 0.31 %.

[Co(TOCO121-H⁺)](NO₃) and [Co(TOCO151-H⁺)](NO₃). Compounds were prepared using a similar procedure as [Co(TOCs-H⁺)](NO₃). [Co(TOCO121-H⁺)](NO₃) was obtained as a pink solid in 60% yield. FT-ICR-MS of [Co(TOCO121-H⁺)-NO₃]⁺ calculated: 518.201216, found: 518.19494. Purity % by ICPMS =96.51%. Co content through ICP-MS calculated for [Co(TOCO121-H⁺)-NO₃]⁺: 10.66%, found: 10.28 % \pm 0.55 %. [Co(TOCO151)](NO₃) was obtained as a pink solid in 68% yield. FT-ICR-MS of [Co(TOCO151-H⁺)-NO₃]⁺ calculated: 572.172950, found: 572.16637. Purity % by ICPMS =94.25%. Co by ICP-MS calculated for [Co(TOCO151-H⁺)-NO₃]⁺: 9.30%, found: 8.77 % \pm 0.35 %.

Magnetic moments. The effective magnetic moments ($\mu_{\rm eff}$) of the complexes were determined by 1 H NMR by using the Evans method (Eqs. 1-3). 35,36 Samples were prepared using a coaxial NMR insert which contained the diamagnetic standard of 5 % t-butanol in D₂O. The outer 5 mm NMR tube contained paramagnetic complexes with fixed concentrations of 4 mM to 8 mM, in the presence of 5 % t-butanol. At least four independently measured values were averaged for each concentration. The mass susceptibility (χ_g) was calculated using Eq. 1, where Δf is the shift in frequency (Hz); ν_0 is the operating frequency of NMR spectrometer (Hz); m is the concentration of the substance (g/mL) and (χ_o) is the solvent correction. The molar susceptibility is obtained by multiplying the mass susceptibility by the molar mass. The paramagnetic molar susceptibility χ_M^p was calculated by subtraction of the diamagnetic susceptibility contribution (χ_M^{dia}) in eq. 2 by using Pascal's constants as reported.³⁷ This result was used to calculate the effective magnetic moment $\mu_{\rm eff}$ (Eq. 3).

$$\chi_g = \frac{3\Delta f}{4\pi v_0 m} + \chi_o$$
 Eq. 1

$$\chi_M^p = \chi_M - \chi_M^{dia}$$
 Eq. 2

$$\mu_{eff} = 2.83 (\chi_M^p T)^{1/2}$$
 Eq. 3

Fluorescence spectroscopy. The samples were dissolved in 500. μ L 1xPhosphate buffered saline (PBS) with milli-Q water in 5 mm quartz cuvette. The samples were excited at the excitation wavelengths of the fluorophore in the complex (Carbostyril λ_{ex} = 330 nm; λ_{max} = 370 nm, Coumarin121 λ_{ex} = 340 nm; λ_{max} = 445 nm and Coumarin151 λ_{ex} = 365 nm; λ_{max} = 490 nm).

Chemical Exchange Saturation Transfer (CEST). The CEST data were acquired at 37 °C with a presaturation pulse power 24 μ T, applied for 2 s at 11.4 T, unless stated otherwise. All samples contained 20 mM (4-(2-hydroxyethyl)-1piperazineethanesulfonic acid (HEPES) buffer in 100 mM NaCl. The frequency offset was varied in 1 ppm (500 Hz) increments, and a CEST spectrum was obtained by plotting normalized water intensity against frequency offset.

¹⁷O NMR spectra. Samples were prepared in water with 1% H₂¹⁷O. The chemical shifts as well as the line width at half-height of the symmetric water peak were determined in the absence and in the presence of metal complex at variable temperatures and pH. The line width at half-height of the signal in absence and in presence of metal complex at variable temperatures was used to calculate the transverse relaxation times using Swift-Connick³⁸ equations.

pH Potentiometric Titrations. Aqueous solutions containing 1.00 mM Co(II) complex in 100 mM NaCl were titrated with an aqueous solution of 90.13 mM NaOH. The 5 μL aliquots of base were added over a period of 60 seconds with an interval of 300 seconds using a Nexus 3000 High Flow Syringe Pump from Chemyx Inc. (Stafford, TX) equipped with a 10 mL Hamilton gastight syringe. During the titration, complex solution was kept under Ar at 25 °C. The changes in pH were monitored from approximately pH 3.26 to pH 12.16. For determination of the protonation states and the pK_a values of the complex from the pH data, the HYPERQUAD 2013 Version 6.0.1 program was used and the speciation diagram was obtained by using the HySS Version 4.0.31 program.

Monitoring of dissociation of complexes by using UV-Vis spectroscopy. Samples were prepared with 50 μ M Co(II) complex and the electronic absorbance was recorded at 330 nm over a period of 6 h at 37 °C. Control samples contained complex with 20 mM HEPES and 100 mM NaCl. The anion stability was determined in presence of 4 mM Phosphate anion and 25 mM carbonate solution. Acid stability samples were incubated with 1.0 mM HCl. Zn(II) displacement assays samples contained 100 μ M Zn(II) in 20 mM HEPES buffer and 100 mM NaCl.

Yeast cultures and labeling. Yeast cells used in the study are *S. cerevisiae of the Sigma1278b* strain background. ³⁹ The specific strain used (PC538) is a typical wild-type (WT) strain with the following genotype: *MATa ste4 FUS1-HIS3 FUS1-lacZ ura3-52*, ⁴⁰ which was used for all experiments in the study. PC538 yeast cells were grown in YEP-GAL [Yeast extract (10g/L), peptone (20g/L), galactose (2%)] liquid media. Yeast cells were grown to midlog phase for about 4h. Cells were harvested by centrifugation, and cell pellets were washed with distilled and deionized water. Harvested control cell pellets were suspended in distilled and deionized water for experiments. For heat treatment, the resulting cell pellet was treated with 50 mM Co(II) complexes in solution in 50% v/v PEG 3350 solution. The cells were incubated at 30 °C for 30 min with continuous shaking. After incubated at 30 °C with continuous shaking for 4 h. The cells were washed with 1 mL 1x PBS and vortexed for 5 s. The mixture was then centrifuged to separate the supernatant and cell pellet. The cells were recovered and resuspended in 1x PBS, pH 7.2. Optical density measurements were done at 600 nm to obtain the cell density to determine the approximate number of cells.

Pierce Protein assay. Cell pellets were collected by centrifugation and stored at -80 °C for 16 h. Cells were thawed to 25 °C and proteins were extracted by the addition of trichloracetic acid (TCA) buffer containing 10% TCA; 10 mM Tris-HCl pH 8, 25 mM ammonium acetate, and 1.00 mM EDTA. Acid-washed

glass beads were added to the scaffold and cell pellet mixture. Cells were lysed by three consecutive 90 s vortex pulses with 1 min rests on ice using the fast prep multi-vortexer (Labline instrument, Melrose, IL). Proteins were precipitated by centrifugation at 4 °C at 16000 g for 10 min. Protein pellets were thoroughly suspended in resuspension buffer containing 0.10 M Tris-HCl pH 11 and 3% SDS by boiling the suspension for 5 min at 95 °C. Total protein concentration was measured using Biorad BCA protein assay kit (Pierce™ Microplate BCA Protein Assay Kit catalog # 23252). The total protein content was plotted against the optical density at 600 nm (OD600). The data was fit to a linear regression graph in graphpad prism.

Fluorescence Microscopy. Cells were washed three times in water and placed on microscopy slides followed by cover slips for imaging by fluorescence microscopy. Fluorescence imaging was done using FITC (Fluorescein Isothiocyanate) channel with exposure 2 s on a Zeiss Axioplan2 fluorescence microscope.

Z-spectra of Co(II) complex labeled yeast cells. Cells were washed three times with 1x PBS. The number of cells was adjusted to obtain 125 μ g/mL of total protein content. Cells were suspended in 1x PBS in 5 mm borosilicate NMR sample tubes. CEST spectra were acquired in a range of \pm 200 ppm by acquiring a total of 321 points (steps of 0.2 ppm in the range of 0 to \pm 20, steps of 1 ppm in the range of \pm 20 to \pm 50 and steps of 5 ppm in the range of \pm 50 to \pm 200 ppm) with B₁ = 12 μ T at 37 °C. The asymmetric analysis was plotted from CEST spectra with the following formula:

Equation 4

$$ST \% = (1 - \frac{MS(\Delta\omega)}{MS(-\Delta\omega)}) \times 100$$

Cell viability assay. Aliquots of control cells, heat treated control cells and complex treated heat treated cells were washed twice with 1x PBS. Serial dilution assays were performed by spotting 10 μ L of serial 10-fold dilutions of cell cultures with optical density OD600 of 0.80 on YEPD [Yeast extract (10g/L), peptone (20g/L), dextrose (20g/L) and agarose (20g/L)] semi-solid agar media. The plates were incubated at 30 °C for 48 h and photographed.

Determination of Co concentration in the yeast cells. The concentration of Fe in the yeast cells was determined by using inductively coupled plasma mass spectrometry (ICP-MS) (Thermo X-Series 2). After the internalization experiments, aliquots of control cells, heat treated control cells and complex treated heat treated cells were collected in 200 μ L distilled deionized water. Yeast cell solutions (100 μ L) were digested with metal free nitric acid (900 μ L) (65-70%). After the etching process, the samples were diluted to 2% HNO₃, in 10 mL distilled deionized water and analyzed by ICP-MS. As the internal standards, cobalt and indium standard solutions were used.

Statistical analysis. Results were expressed as mean value ± standard error (SE). Statistical analyses were performed using one-way ANOVA analysis followed by Tukey's multiple comparisons test by using Graphpad Prism 8. A P value of less than 0.05 was regarded as significant for cell uptake and viability studies.

Results

Design and Synthesis of the Complexes. The four macrocyclic ligands with 1,4,7-triazacyclononane (TACN) framework were synthesized by monoalkylation with the modified fluorophore to produce an intermediate that was extracted into organic solvent (Scheme S1-S2). The three fluorophores were added through an amide linkage that would coordinate to the Co(II) through the

carbonyl group. Carbostyril, Coumarin121 and Coumarin151 were investigated as fluorophores to append to the amide group, as reported previously for ligands used in lanthanide complexes. ^{41, 42} TOCs and TACs has carbostyril, TOCO121 has Coumarin121 and TOCO151 has Coumarin151 as the fluorophore. Two hydroxypropyl pendants or two amide pendants were added subsequently to provide exchangeable protons for CEST. Previous research in our group suggested enhanced second sphere interactions via hydrogen bonding to hydroxypropyl pendant groups in particular, which could potentially increase water interactions to produce increased water proton hyperfine shifts. Moreover, hydroxyl pendants increase solubility, which is potentially a concern when the third pendant is a fluorophore containing an aromatic group. ³²

Studies here focused on macrocycles and complexes with hydroxypropyl pendants (Scheme 1). The complex with amide pendants, Co(TACs), was prepared primarily for aid in the assignment of CEST peaks (Scheme S2). Co(NO₃)₂ was added to an ethanolic solution of ligands to prepare the Co(II) complexes which were isolated as light pink solids to give complexes with surprisingly high solubility (50 mM at neutral pH). High solubility is an important property for complexes used as cellCEST agents in order to produce hyperfine shifted proton resonances of cellular water or other components.

Characterization of complexes. Given that there are multiple ionizations and multiple solution species for the three Co(II) complexes, we designate a general label for any species (Co(TOCs), Co(TOCO121), Co(TOCO151) or Co(TACs) as shown in Scheme 1. Designations are given as needed for specific species. For example, Co(TOCs-H⁺) is a complex species with a singly deprotonated ligand.

The electronic absorbance and fluorescence properties of all hydroxypropyl containing ligands and their Co(II) complexes were characterized. The complexes exhibited the characteristic absorbances and fluorescent properties of the fluorophore involved. The Co(TOCs) complex has carbostyril as the fluorophore which shows two vibronic bands at 325 nm and 340 nm.⁴² Co(TOCO121) and Co(TOCO151)

have coumarin121 and coumarin151, respectively, as fluorophores. Both coumarin fluorophores show broad absorbances with peaks at 325 nm and 345 nm respectively (Figure S4).⁴²

The coumarin fluorophores have large Stokes shift in comparison to the carbostyril fluorophore (Figure 1). The larger Stokes shift in the coumarin fluorophores are attributed to the push-pull effect between the electron rich 7-amino group and electron deficient coumarin core. ⁴³ Fluorescence quenching was observed in the complexes compared to the free parent fluorophores as shown for Co(TOCO121) (Figure S1). The fluorescence quenching likely results from photoinduced electron transfer (PET) from the paramagnetic center to the excited state of the fluorophores. Further, quenching of the fluorescence due to aggregation of this complex at concentrations above 50 µM is likely (Figure S1b). Low fluorescence quantum yields of a few percent are, in fact, desirable for a bimodal agent since MRI applications require relatively high (millimolar) concentrations of these complexes. Quenched fluorescence would allow for cellCEST relevant concentration loading without compromising the detection of these agents by fluorescence spectroscopy. The desired fluorescence quantum yield also depends on the sensitivity of the fluorescence detector to the emitted light, as studied here by epifluorescence microscopy. Unfortunately, the excitation wavelengths of the fluorophores used here were in the UV and not compatible with a standard confocal microscope.

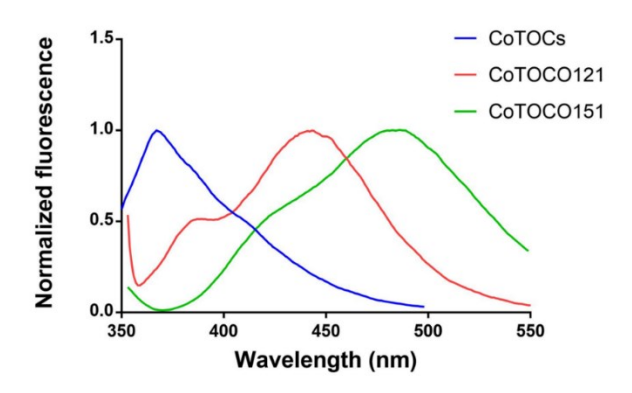


Figure 1. Normalized Fluorescence emission spectra of (i) 50 μ M Co(TOCs) (blue) with λ_{ex} = 330nm. (ii) 50 μ M Co(TOCO121) (red) with λ_{ex} = 345nm. (iii) 50 μ M Co(TOCO151) (green) with λ_{ex} = 365nm. The solutions were prepared in HEPES buffer (pH 7.2) and 0.1 M NaCl at room temperature.

Solution Speciation by pH-potentiometry and UV-vis Spectroscopy. The solution speciation of Co(TOCs) and Co(TOCO121) was investigated by using pH potentiometric titrations to determine the equilibrium constants for deprotonation of alcohol, aromatic amide or water ligands (Figure S2-S3). As given in Table S2, two different ionizations were observed for Co(TOCO121), one with a low pK_a value (5.9) and one with a high pK_a (10). We assign the lower pK_a to the aromatic amide proton based on pH dependent changes in the electronic absorbance spectra of the appended fluorophore as described below. In addition, previous studies of nine-coordinate Ln(III) complexes with analogous pendant dyes linked through bound amide pendants have pK_a values of 7.7-9.5.⁴² Moreover, the similarity of the changes observed in the pH dependent NMR spectra of all four complexes, including the complex with all amide pendants, suggests that it is the amide connected to the dye that deprotonates. The group with the higher pK_a value is attributed to a hydroxypropyl group or, alternatively a bound water. Analogous Co(II) complexes with two hydroxypropyl pendants have OH groups that ionize with pK_a values of greater than 8.0.³²

Three different ionizations were observed for Co(TOCs). The two p K_a s of most interest, at 5.9 and 6.7 are attributed to the aromatic amide NH group based on the changes observed in the electronic absorbance spectra and the NMR spectra. The second p K_a is assigned to a hydroxypropyl OH or water ligand, based on literature values for Co(II) complexes of triazacyclononane.⁴² The ionizations are not attributed to the ring NH group, based on literature values for carbostyril dyes.⁴² The high p K_a at 10.4 is assigned to either a hydroxyl pendent group or a water ligand. The speciation diagrams for Co(TOCs) and Co(TOCO121) are shown in Figure S3.

To further explore the effect of ionization on solution properties, the electronic spectra for Co(TOCs), Co(TOCO121) and Co(TOCO151) were recorded over the pH range of 4 to 8. The changes in these UV-vis spectra with change in pH were substantial. The lack of an isosbestic point for Co(TOCs) over the range of 4.0 to 7.5, is consistent with greater than two species in solution under these conditions

(Figures S5-S7). The absorbance peaks for Co(TOCO121) and Co(TOCO151) undergo a red shift over this pH range. Electronic spectra for Co(TOCO121) at millimolar concentrations show absorbances at 510-520 nm that are assigned to d-d transitions (Figure S8). Increasing the pH from 3.8 to 7.3 produces minimal differences in the absorbance spectrum in this region, consistent with the absence of donor group changes in the coordination sphere. The original spectrum is recovered upon adjustment of the pH of the solution back to acidic pH, supporting reversible pH induced changes in speciation.

NMR Spectroscopy Studies. The Co(II) complexes were characterized in solution by measuring the effective magnetic moment using Evans method. The effective magnetic moments for the complexes (4.23-4.46) were consistent with high-spin Co(II) (Table S1). The ¹H NMR for all three complexes displayed relatively sharp and highly shifted proton resonances at 25 °C which are characteristic of high-spin Co(II) complexes (Figure S9). Moreover, a similar pH dependent shift in the ¹H NMR spectrum was observed in the three hydroxypropyl containing complexes (Figure S10-S11 and S13). The pH dependence of the ¹H NMR resonances spectra coincide with ionization of a donor group over the pH range of 4.0 to 7.5.

The ¹H NMR spectra of all three Co(II) hydroxypropyl-containing complexes under acidic conditions exhibited resonances that span the range of -100 ppm to + 240 ppm. For Co(TOCs) and Co(TOCO121) there were nineteen distinct proton resonances in the paramagnetic region. The resonance at -5 ppm was found to be of six-fold intensity and was assigned to the methyl groups on the hydroxypropyl pendants. The spectrum consisted of seven broad and twelve sharp resonances for both complexes. Comparison with the previously reported Co(TOT) complex (Scheme S3, Figure S14) suggests the resonances at 40, 20, 13, 11 and 7 ppm are from the amide appended fluorophore. The relative equivalence of 4 protons on the fluorophore core suggests the absence of geometrical isomerism due to the two possible conformers that would result from the C-N double bond in the aromatic amide at acidic pH as shown in Scheme 2. Notably, several proton resonances are slightly broadened while the

remainder are sharp, suggesting that the complexes are fluxional under these conditions. The similarity of the ¹H NMR spectra of the Co(II) complexes studied here with Co(TOT) (scheme S3, Figure S14) suggests that the complexes have similar coordination geometry. Thus, we propose that the complexes are six-coordinate with all three nitrogens from the TACN macrocycle, two hydroxypropyl donors as well as the carbonyl group from the aromatic amide are all bound to Co(II). Co(II) complexes of TACN with hydroxypropyl pendants are shown to have distorted trigonal prismatic geometry.⁴⁴

For Co(TOCO151), a total of sixteen proton resonances were observed under acidic conditions (Figure S9). Out of these, 15 integrate to approximately the same intensity and a peak at -4.6 ppm corresponds to methyl groups on the hydroxyl pendants with six-fold higher intensity. The spectrum consisted of seven broad and nine sharp resonances in the case of Co(TOCO151) with the amide appended fluorophore peaks at 40, 20, 13 and 11 ppm. The absence of a peak at 7 ppm, assigned to the methyl in Co(TOCO121), in the spectrum of Co(TOCO151) suggests the peak belongs to the methyl group in the TOCO121 fluorophore (Figure S17). The 4-methyl peak in the free dyes carbostyril and coumarin121 fluorophore generally appears at 1.1 ppm. The downfield shift of the methyl protons is indicative of the proximity of the fluorophore to the Co(II) center at acidic pH. Similar to the other complexes, the number of proton resonances support a single diastereomer under acidic conditions for Co(TOCO151).

The ¹H NMR spectra of all three hydroxypropyl containing Co(II) complexes at neutral pH exhibited more highly shifted and sharper resonances (Figure S10 – S11 and S13). The ¹H NMR spectra spans the range of -120 ppm to + 260 ppm for all three complexes. Interestingly, the spectra displayed striking similarity to Co(TOB), a complex with only two hydroxypropyl pendants and at least one bound water (Scheme S3, Figure S15). Seventeen proton resonances were observed for Co(TOCs) whereas twenty-one proton resonances of unequal integration were observed for both Co(TOCO121) and Co(TOCO151) at 25 °C (Figure S10-11 and S13). Two resonances, one at 6 ppm and one at -12 ppm with three-fold greater intensities were assigned to the two methyl groups on the alcohols in all three complexes. In all, twenty-

one non exchangeable protons were observed in the case of Co(TOCs) and twenty-two non-exchangeable protons in the spectra for Co(TOCO121) and Co(TOCO151). Variable temperature ¹H NMR studies of Co(TOCO121) showed that the proton resonances sharpened upon increase in temperature to 60 °C, and several new resonances assigned to the fluorophore appeared at this higher temperature (Figure S12). Thus, we attribute the lack of aromatic resonances of the fluorophore at room temperature to broadening associated with dynamic processes. The resonances at 66, 59, 34.5, 16 and 7.8 ppm were attributed to the fluorophore protons upon comparison with the ¹H NMR of Co(TOB) (Figure S15).

By comparison, the ¹H NMR of the Co(TACs) complex shows only six paramagnetically shifted resonances over the range of 240-7 ppm. The small number of resonances as well as their large peak width supports the dynamic nature of the complex, similar to that observed with analogous Co(II) complexes with amide pendants (Figure S18).^{33, 45} At neutral pH, the number of paramagnetically shifted proton resonances doubles, consistent with the formation of a more rigid complex that is most likely a single diastereomeric form.

Variable Temperature ¹⁷O NMR Spectroscopy. To characterize the interaction of these complexes with bulk water, variable temperature ¹⁷O NMR studies were carried out. The ¹⁷O NMR spectra were collected every 5 °C at temperatures ranging from 25 to 80 °C. Variable temperature ¹⁷O NMR studies on Co(TOCO121) at pH 3.4 and 7.0 (Figure 2) enabled us to characterize the effect of pH on the water exchange.

Interestingly, all four complexes displayed substantially broadened and shifted 17 O resonances of water at pH 6 and above (Figure S19-22). The broadening and shifting of the 17 O resonance of water supports the presence of inner-sphere water. $^{46, 47}$ The order of broadening and shift of the 17 O resonance was: Co(TOCO151) > Co(TOCO121) > Co(TOCs) > Co(TACs) at temperatures between 35 °C and 45 °C. The transverse relaxation time (T_{2r}) and the reduced chemical shifts ($\Delta\omega_r$) of the Co(II) complexes were

recorded as a function of temperature (Table S4-S7). These data were fit to Swift-Connick equations as reported in the literature.³² At pH 6, all four complexes displayed a plot of the $ln(1/T_{2r})$ versus inverse temperature that are characteristic of an exchangeable inner-sphere water (Figure S25-S28, Figure 2). This data was fit to give k_{ex} rate constants for water on the order of 10^6 to 10^7 s⁻¹. At near neutral pH, all complexes transitioned from fast exchange to slow exchange at around 35 °C (Figure S23).

In contrast, barely any shift or broadening of 17 O water resonance was observed for Co(TOCO121) at acidic pH (Figure 2), consistent with no inner-sphere water under these conditions. The observed curve in the plot of $ln(1/T_{2r})$ versus inverse temperature may be due to a fractional bound water or to a tightly bound second-sphere water as observed previously for analogous complexes such as Co(TOT).

The water ¹H hyperfine shift, corrected for bulk magnetic susceptibility effects, was plotted as a function of concentration for all three complexes at both acidic and neutral pH (Figure S29, Table S9). All three complexes displayed significant enhancements in ¹H water shift at neutral pH compared to acidic pH, supporting the presence of an exchangeable inner-sphere water a near neutral pH, but not at acidic pH. The ¹H water shifts at neutral pH however, were smaller than the values observed for other Co(II) macrocyclic complexes with amide or alcohol donors. ^{33, 34} Water proton hyperfine shifts are attributed to a combination of inner-sphere and second-sphere interactions of the paramagnetic complex with water. In addition, hydroxypropyl pendants are known to be involved in strong second sphere water interactions through hydrogen bonding. ³²

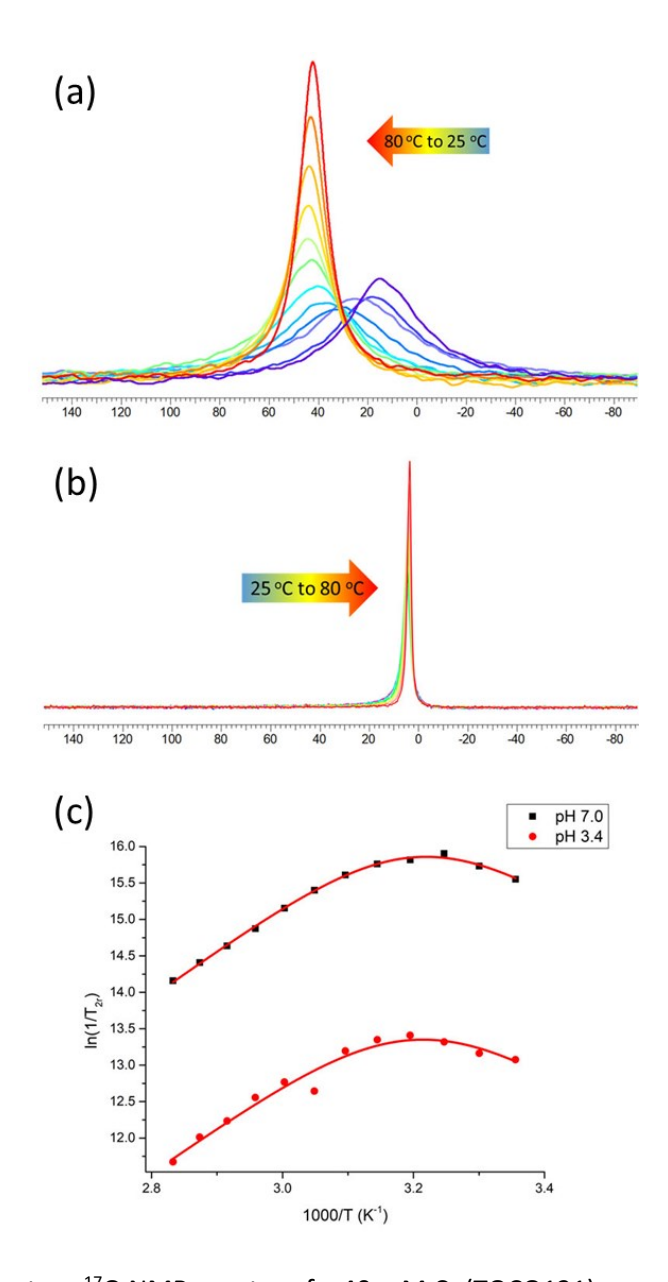


Figure 2. Variable temperature 17 O NMR spectra of a 40 mM Co(TOCO121) sample in 1% $\rm H_2^{17}O$ at (a) pH 7.0 and (b) pH 3.4 from 25 to 80 $^{\rm o}$ C. (c) Transverse 17 O relaxivity, $\rm ln(1/T_{2r})$, as a function of temperature for 40 mM Co(TOCO121) at pH 7.0 (black squares) and pH 3.4 (red circles).

Chemical Exchange Saturation Transfer (CEST) Studies. Z- spectra were recorded to examine the CEST effect and were plotted as the percent reduction of the bulk water peak, as a function of the presaturation frequency at 1 ppm increments for all four Co(II) complexes.⁴⁵ As expected from the ¹H NMR spectra, all three hydroxypropyl containing Co(II) complexes displayed pH dependent CEST peaks

(Figure 3(a)-(c), S30-32). The change in the position and intensity of the CEST peaks with change in pH was quite dramatic over the pH range of 4-8. In general, the number of CEST peaks was larger at acidic pH than at neutral or basic pH and the CEST peaks were more intense at near neutral pH. Out of the three complexes, Co(TOCO121) consistently displayed the strongest CEST signal.

At acidic pH, complexes with the coumarin fluorophore displayed three CEST peaks of low intensity whereas carbostyril appended Co(TOCs) exhibited a fourth CEST peak at 21 ppm. The peak at 21 ppm that was observed for Co(TOCs) is tentatively assigned to the amide proton from the quinolinone core of the carbostyril fluorophore as it does not shift substantially but increases in intensity as pH is increased to 7.3, then decreases. Apart from the extra peak in Co(TOCs), the remainder of the CEST peaks were found to be in similar positions. The farthest shifted peak was observed at 200 ppm in Co(TOCO151), 197 ppm in Co(TOCO121) and 187 ppm in Co(TOCs) (Figure 3 (a)). These highly shifted peaks are advantageous for paraCEST agents, although the peaks are of rather low intensity. The other broad peak was found between 75-85 ppm along with a slightly sharper peak at 33 ppm.

The peaks displayed an increase in intensity upon titration from pH 4 to pH 6.5, before broadening followed by disappearance of the peak. The increase in intensity with pH is characteristic of base catalyzed proton exchange that would be expected to increase peak intensity. The change in the position of the CEST peaks between pH 6 to pH 6.5 is consistent with the ¹H NMR spectral changes with pH and is attributed to a substantial change in geometry due to addition of an inner sphere water upon deprotonation of a ligand donor group.

At neutral pH, Co(TOCO151) and Co(TOCO121) displayed similar CEST spectra with two peaks whereas, Co(TOCs) displayed three CEST peaks (Figure 3(b)). The third peak in Co(TOCs) was in a similar region as that assigned to the quinolinone proton in the carbostyril core of the fluorophore. The farthest shifted peaks were at 112 ppm for Co(TOCO151), 105 ppm for Co(TOCO121) and at 97 ppm for Co(TOCs).

The less highly shifted peaks were at -18 ppm for Co(TOCO151), -20 ppm for Co(TOCO121) and at -25 ppm for Co(TOCs). The two shifted CEST peaks are attributed to hydroxypropyl OH groups that are in different environments. As shown above, the water ligand exchanges too rapidly to produce a CEST effect. Assignment of these peaks is discussed further below.

The pH dependent change in CEST spectrum was plotted and used to estimate the ionizations of the respective complexes (Figure 3(d), S34-35). The changes observed in the CEST peak intensity was in general agreement with the observed values through pH potentiometrics (Figure S2, Figure S34). The most pronounced changes in intensity were between pH 6 and 7.

The Z-spectrum of the Co(TACs) complex showed several weak CEST peaks that were not highly shifted from the bulk water peak (Figure S33). No CEST peaks were detected at pH 4.6, unlike the three hydroxypropyl complexes. All peaks increased in intensity over the pH range of 6.0 to 7.0, consistent with base catalyzed NH proton exchange. At pH 7.6, the most prominent CEST peak was at 44 ppm. The peaks are assigned as NH protons of carbostyril ring at 21 ppm, carbostyril amide linker at 33 ppm and the amide pendant groups at 44 ppm. In comparison, the symmetric Co(II) complex of TCMT (1,4,7-tris(carbamoyl)-1,4,7-triazacyclononane) shows a single CEST peak at 32 ppm.⁴⁵ This support the assignment of the furthest shifted CEST peaks of Co(TOCs), Co(TOCO121) and Co(TOCO151) as the OH groups of the hydroxypropyl pendants.

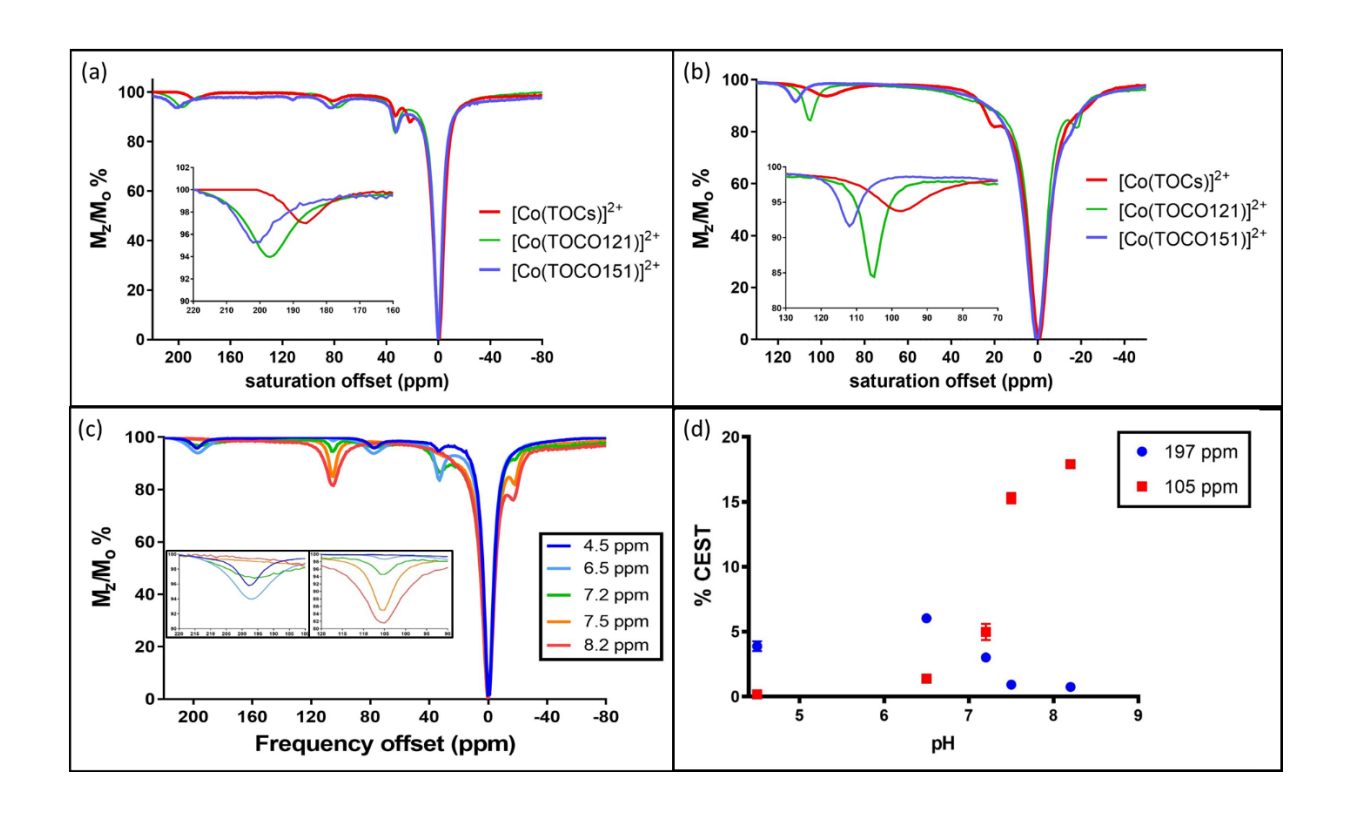


Figure 3. CEST spectra at (a) pH 6 and (b) pH 7.5 for Co(TOCs), Co(TOCO121) and Co(TOCO151) at 37 °C. Samples contained 20 mM complex, 20 mM buffer MES, 100 mM NaCl with B_1 = 1000 Hz (24 μ T) applied for 2s. (c) CEST spectra of Co(TOCO121) at 37 °C showing pH-dependence and (d) Plot of CEST % with pH of CEST peaks in Co(TOCO121).

Dissociation of Complexes. The macrocyclic framework encapsulates the Co(II) center to provide control of spin and oxidation state and to prevent reactions that might be observed with an open coordination site for binding water.⁴⁸ In addition, these macrocycles enhance the kinetic inertness towards release of Co(II) for the complex. All three Co(II) complexes displayed little change in UV-Vis absorption at the fluorophore over a period of 12 h when challenged in the presence of biologically relevant anions and acid at biologically relevant concentrations (Figure S36-38). Co(TOCs) and Co(TOCO151) displayed no detectable change in absorbance in the presence of acid, biologically relevant anions and equimolar amounts of Zn(II). Co(TOCO121) showed the least dissociation with little change in absorbance in the presence of acid, anions, or equimolar Zn(II). The lack of change or drop in absorbance mitigates against amide bond hydrolysis and subsequent release of the free fluorophore as well as the

dissociation of Co(II). Further, pH titrations monitored by UV-vis spectroscopy of the Co(TOCO121) d-d transitions showed that pH-induced absorbance peak changes were reversible (Figure S8). These data show that the complexes are robust towards dissociation when challenged with acid or competing anions or cations.

Labeling of Yeast and cellCEST studies. Yeast cells were grown to mid log phase from a saturated culture to ensure a rapidly dividing population of healthy cells. Due to necessity of using long wavelength UV excitation and emission of Co(TOCs), this compound was not used in the cell studies. Initial attempts to induce cell uptake through simple incubation of complexes with the cells were not successful. Heat treatment transformation was used to enhance the uptake of complexes into the cells.⁴⁹ Assays to determine total protein levels were performed on the cells to determine the relationship between total protein content and optical cell density (Figure S41).⁵⁰ Optical densities were adjusted with respect to total protein content of the cells, to normalize the cell samples for various experiments.

Cell labeling studies were carried out by using fluorescence microscopy to screen conditions and quantitated by using ICP-MS analysis. The incubation time of yeast with the complex upon heat treatment was studied by using fluorescence microscopy for Co(TOCO151) (Figure S42). Total corrected fluorescence intensity measurements on the fluorescence images suggested 4 hours was the optimal time for the maximum cell association (Figure S43). However, we note that aggregation of the Co(II) complex may make it challenging to use fluorescence to quantitate cell association or uptake. After treatment with the Co(II) complexes, the cells were collected and washed with 1x PBS buffer and imaged by fluorescence microscopy. Fluorescence was observed in the FITC channel with an exposure of ~2 s. The heat treated cells incubated with both Co(II) complexes exhibited fluorescence enhancement in the FITC channel compared to heat treated untreated control cells (Figure 4). Both complexes displayed a localized punctate pattern, suggesting that cell labeling may be associated with secretory pathway mediated

uptake. The image is blurred by background fluorescence, but does appear punctuate compared to previous studies of an analogous Fe(III) complex that showed more diffuse cellular fluorescence images.²⁷ Such punctuate staining is similar to that observed for uptake with DNA payloads for heat treatment transformations.⁴⁹

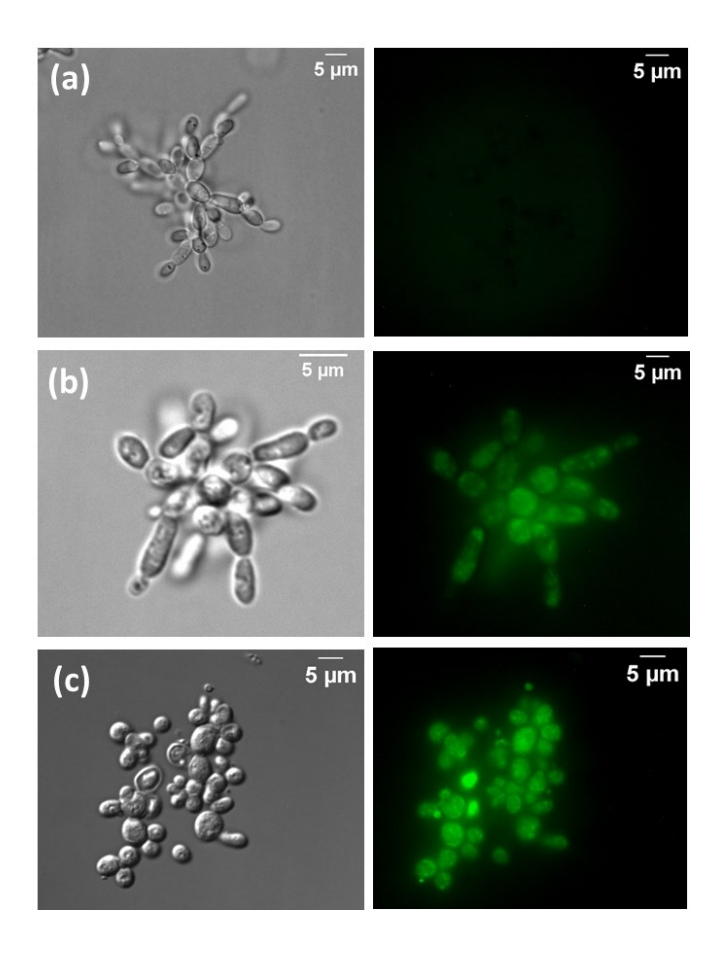


Figure 4. Fluorescence microscopy images of S. cerevisiae PC538 cells. (a) control cells (b) Co(TOCO121) (50 mM) treated heat treated cells and (c) Co(TOCO151) (50 mM) treated heat treated cells. Excitation (470 nm) emission (509 nm). All examples show fluorescence with 5 μ M scale and exposure 2 s.

The complex labeled cells and control cells were harvested and suspended in 1x PBS. These cell samples were normalized with respect to the total protein content of 125 μ g/mL and transferred to NMR tubes for CEST experiments. The Co(II) complex labeled cells produced broadened CEST spectra with slight asymmetry (Figure 5(a)). In the case of both Co(II) complex labeled samples, a broader CEST signal is

detectable. Due to the cellular loading of paramagnetic metal there is an overall decrease in T2* leading to a broad CEST spectrum.²² The percentage saturation transfer (ST%) was plotted using equation 4 (Figure 5(b)). For both control and heat treated control cells, a signal between 1 to 2 ppm is present due to endogenous exchangeable protons with maximum saturation transfer between 25-30% at 1 ppm. The Co(II) complex labeled cells displayed a broad saturation transfer in the range from 1 to 4 ppm. In the case of Co(TOCO151) labeled cells, the maximum of saturation transfer was at 1.6 ppm at 15%. Despite the broad central peak in Co(TOCO121) labeled cells, only a small saturation transfer offset was observed. The marginal shift in the intracellular exchangeable proton resonances in yeast cells is attributed, in part, restricted water exchange through the thick yeast cell wall. Alternatively, we cannot discount oxidation of the Co(II) complexes to Co(III) or other reactions that would quench the paramagnetism of the complexes upon association with the yeast cells.

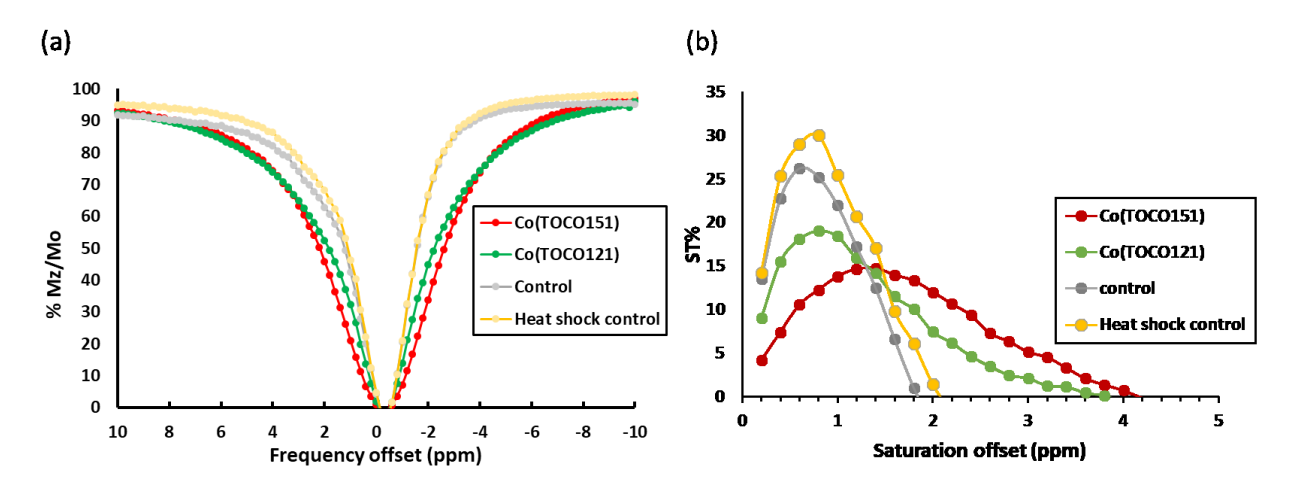


Figure 5. (a) Z-spectra of cell suspensions and (b) Saturation transfer spectra of Co(TOCO151) (50mM) treated heat treated cells, Co(TOCO121) (50mM) treated heat treated cells, untreated control cells and untreated heat treated cells with $B_1 = 12 \mu T$. All the samples contain 125 $\mu g/mL$ protein.

The association of Co(II) complexes was measured by using ICP-MS measurements of total cobalt content in the cells (Figure 6). Both Co(TOCO121) and Co(TOCO151) labeled cells exhibited significantly higher cobalt content compared to untreated control and heat treated control cells. These results were

in agreement with the fluorescence uptake studies. Co(TOCO151) treated cells displayed higher association of complex compared to Co(TOCO121), which corresponds to a slightly more pronounced cellCEST effect.

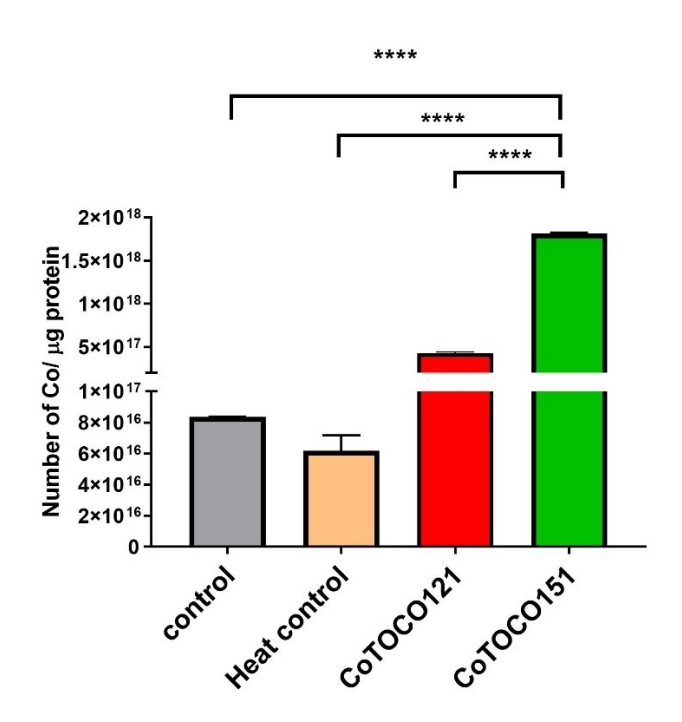


Figure 6. Total cobalt content in yeast cells measured by ICP-MS. Mean \pm SE is reported, (****) p<0.0001, n=3 for Control, Heat treated Control, Co(TOCO121) and Co(TOCO151).

Serial dilution assays were performed to assess the cell viability of Co(II)-complex treated cells (Figure S44). Unfortunately, both complexes exhibited severe toxicity compared to untreated control cells. Co(TOCO121) was marginally less toxic than Co(TOCO151), which might result from lower cellular association of Co(TOCO121). Lowering the concentration of the Co(II) complexes in the heat shock treatment did not produce a discernable cellCEST effect in z-spectra of suspended yeast, so no further studies were pursued under these conditions. These data suggest that the cobalt labeled yeast cells will not be sufficiently viable for cell tracking studies.

Discussion

The three Co(II) complexes with hydroxypropyl pendants show remarkable solution properties including good aqueous solubility and a pH dependent change in speciation that produces the largest shift in CEST peaks that we have observed to date. The pH dependence of NMR spectra, CEST spectra, electronic absorbance peaks of the dyes in conjunction with pH-potentiometric data support a group that ionizes with a pKa at slightly acidic pH. Comparison to the solution chemistry of related complexes including Co(TOT), Co(TOB), Co(DCMT) and Co(TCMT) suggest that the fluorophore bearing pendant plays a role in the unusual pH dependent CEST properties. Data are most consistent with deprotonation of the amide linker connecting the fluorophores to the macrocyclic complex as shown in Scheme 2. Notably, binding of metal ions to amide pendants gives rise to an increase in the resonance structure with a CN double bond as shown below.^{11, 51} Another alternative, binding through the nitrogen of the amide linker has been observed for a Co(III) complex.⁵² However, the Co(II) complexes studied here show a reversible pH promoted change which is inconsistent with the formation of Co(III). Moreover, the d-d transitions of Co(TOCO121) do not change markedly, consistent with a similar coordination sphere at acidic and neutral pH. At neutral pH but not acidic pH, ¹⁷O NMR studies are consistent with the presence of a bound water for all four Co(II) complexes. Such seven-coordinate complexes are fairly common in Co(II) macrocyclic coordination chemistry.³²⁻³⁴ The exchangeable inner-sphere water is expected to produce large bulk water proton shifts.

Scheme 2

The Co(II) complexes with hydroxypropyl pendants display several highly shifted CEST peaks. At acidic pH, three CEST peaks between 187-200 ppm, 75-85 ppm and a sharper peak at 33 ppm were observed. The low intensity of the peaks and the large range that they span are characteristic of hydroxyl OH groups bound to Co(II).³² The most highly shifted peaks between 187-200 ppm in the complexes were broad and had relatively low intensities (<5% saturation transfer for 20 mM complexes at pH 6). Most likely the two furthest shifted peaks are OH CEST peaks. This assignment is supported by the lack of highly shifted CEST peaks in the amide complex, Co(TACs). The third and least shifted peak is assigned to the amide NH. Notably, the restricted rotation about the CN amide bond in the dye-bearing pendent might give different isomers, but data is most consistent with a single geometric isomer. For Co(TOCs), an additional CEST peak at 21 ppm was observed at acidic pH and was attributed to the amide proton from the quinolinone core of the fluorophore. Plotting the magnitude of saturation transfer of the CEST peaks at 187-200 ppm and 97-112 ppm versus water with pH, were consistent with ionizations at slightly acidic pH values for Co(TOCs), Co(TOCO121) and Co(TOCO151).

Comparisons can be drawn with other TACN based Co(II) complexes.³² Co(TOT) has a highly shifted CEST peak attributed to the OH of hydroxypropyl pendants that appears at 140 ppm, in a similar but not as highly shifted position to the CEST peaks of the complexes here as studied at acidic pH. The CEST peak positions of OH protons of hydroxypropyl pendants of Co(II) complexes is, however, highly variable. The Co(TOB) complex, containing two hydroxypropyl pendants, a bound water and one benzyl group, has a single CEST peak at only 37 ppm. Thus, while it is quite remarkable to have two CEST peaks one at 187-200 ppm and 75-85 ppm that are assigned to OH groups, the variable chemical shifts observed for OH protons of hydroxypropyl pendants in Co(II) complexes supports this assignment. The third donor group proton that produces CEST at about 30 ppm is tentatively assigned as the amide NH.

At neutral pH, the two CEST peaks that are observed for the three hydroxypropyl complexes including the most shifted ones at 97-112 ppm and the least shifted at -10 to -25 ppm are tentatively assigned to hydroxypropyl OH groups in the complexes containing a deprotonated amide group and a bound water. The inner-sphere water in the seven-coordinate complex exchanges too rapidly to produce a CEST peak. The proton exchange rate constants displayed a pH dependent increase ranging from 500 s⁻¹ to 3500 s⁻¹ for all the major CEST peaks which is typical of base catalyzed exchange for amide NH or hydroxyl OH. The larger magnitude of the CEST peaks at basic pH is attributed, in part, to the higher concentration of hydroxide to catalyze rapid proton exchange.

To assess the stability of the complexes prior to applications in cellular studies, the resistance of these Co(II) complexes to dissociation was monitored using UV-Vis spectroscopy in presence of biologically relevant cations and anions. The complexes were also treated with acid. All three complexes showed a small amount of dissociation in the presence of biologically relevant anions, equimolar Zn(II) or under acidic conditions. This resistance to dissociation also supports coordination of all pendants to the Co(II) center.

For the design of the paraCEST agents for cellCEST applications, the exchange rate (k_{ex}) across the membrane in relation to the water shift ($\Delta\omega$) is of great importance for optimum saturation transfer. ^{5,9,53,54} The water exchange across the membrane should be slow enough for the intracellular water to be sufficiently paramagnetic and fast enough to contribute to the saturation transfer to bulk water. Due to similarity of concepts between cellCEST and lipoCEST, the following equations can be used in context of cellCEST:

$$\Delta\omega = 2\pi. \left| \delta^{bulk \ water} - \delta^{intraliposomalwater} \right|$$

$$\delta^{intraliposomalwater} = \delta_{DIA} + \delta_{BMS} + \delta_{HYP}$$

Where δ_{DIA} is the diamagnetic contribution, δ_{BMS} is the bulk magnetic susceptibility contribution and δ_{HYP} is the hyperfine contribution. The BMS contribution is dependent on the shape and orientation of the paramagnetic agent labelled vesicle, the effective magnetic moment (μ_{eff}) and concentration of the paramagnetic center. The choice of cells is critical for the success of the cellCEST. Red blood cells (RBCs) due to their characteristic biconcave shape have exhibited the most far shifted and efficient saturation transfer. ^{22,55} In this regard, yeast cells could also potentially enhance the BMS contribution due to their ellipsoidal shape. Furthermore, cell shape changes can be induced in *S. cerevisiae* by exposure to various environmental stressors that triggers filamentous growth. ⁵⁶⁻⁵⁹ In addition, yeast cells have impressive osmotolerance (growth in 1M KCI, for example) and can be coerced to take up large amounts of metal complex. ^{60,61}

The dipolar water shift ($\Delta\omega$) also depends on the concentration of the internalized contrast agent; thus the paraCEST agent must be optimally concentrated within the cells. Fluorescence spectroscopy is a highly sensitive and non-invasive imaging modality. The fluorophore tag in the paraCEST agents has two purposes. First, the fluorophore is important in optimization of cell uptake conditions and secondly for non-destructive assessment of the localization of the paraCEST agents in cellular compartments. In this

study three Co(II) complexes with three different fluorophores were synthesized to track cell association and uptake. As expected, the photophysical properties were found to be similar to the parent fluorophore although highly quenched compared to free ligand.^{27, 42}

S. cerevisiae cells were labeled with Co(TOCO121) and Co(TOCO151) using the heat treatment transformation protocol with about 50 mM complexes. 62 As a result, labeling in the range of 10¹⁰-10¹¹ Co/cell was observed through ICP-MS analysis of the labeled cells. These values were comparable to the metal content achieved in Ln-based complexes in mammalian cells. 21-23 Notably, large amounts of metal ion can associate with yeast cells.²⁷ The Co amount in the control cells was at least one order of magnitude lower than the Co(II) complex labelled cells (Figure 6). Assuming yeast cells to be spherical in shape with diameter in the range of (5±2) µm, the estimated cell concentration of these complexes was calculated to be between 1.4-17.6 M and 0.3-4 M for Co(TOCO151) and Co(TOCO121) respectively.²⁷ Despite the high concentration of complex associated with the cells, the extent of saturation transfer observed was disappointing. The small water shift that was observed despite the proven ability of the complexes to show water proton shift is consistent with the sequestering of the agents within organelles, leading to the lack of exchange of the paramagnetically labeled intracellular water. It is also possible that the Co(II) complexes had decreased paramagnetic shifts through reduction to diamagnetic Co(III). However, similar effects showing a loss of water exchange were observed when Fe(III) analogs of these complexes as T₁ shortening agents were internalized in yeast cells.²⁷ It is evident from the punctate pattern observed by fluorescence microscopy that the complex may be trapped in the secretory pathway along with cytosolic distribution. This behavior is in accordance with the mechanism of cell uptake enhancement through heat treatment transformation observed in S. cerevisiae. 49 The mechanism of saturation transfer in case of organeller entrapment, would require the water molecule to cross the membrane of the internal organelle as well as the cell membrane and cell wall (Error! Reference source not found.). The detrimental effect of endosomal entrapment on the saturation transfer has been reported in the literature.⁶³

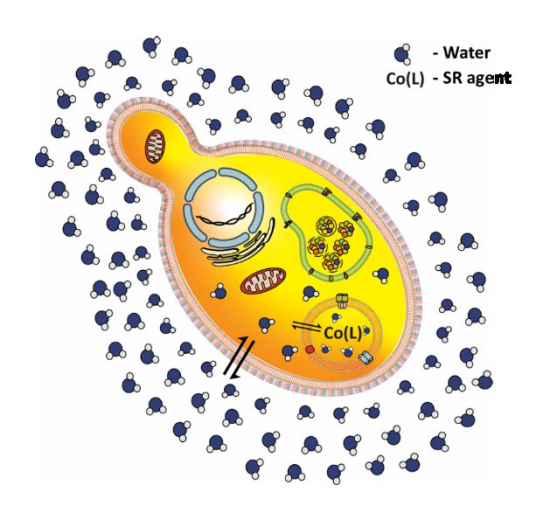


Figure 7. Schematic representing compartmentalization of Co(II) shift agent in *S. cerevisiae* yeast.

One way to modulate the cellCEST effect is to enhance the cell wall interaction between paramagnetic complex and yeast instead of promoting internalization of the complex. We have recently reported association of coordinatively unsaturated Fe(III) complexes to nanoparticles formed from the yeast cell wall²⁸ and also with *S. cerevisiae* and *C. albicans* upon incubation with the Fe(III) complexes. Such interactions have an effect on the Z-spectra, perhaps by affecting the exchangeable OH groups of the β -glucan polymers to give a supramolecular CEST effect, but are dominated by T₂ effects. The Co(II) complexes did not show strong proclivity towards the β -glucan present in the cell wall and there was no detectable association upon incubation. However, long alkyl chains have been used to anchor Gd(III) based contrast agents to yeast derived nanoparticles.⁵ A similar approach may be useful here for Co(II) complexes and may lead to lowered concentrations of Co(II) complex at doses that do not harm the cells.

Conclusions

In summary, four Co(II) based bimodal imaging agents were synthesized with the goal of observing cellCEST in *S. cerevisiae*. The Co(II) complexes with hydroxypropyl pendants displayed unusual pH

response as shown in CEST spectra that are attributed to changes in coordination sphere arising from ionization of the amide NH group on the fluorophore linker. Aromatic amide groups have not been commonly studied as donor groups in transition metal ion paraCEST agents. The application of the Co(II) complexes as pH sensors was not pursued due to the low intensity of the CEST peaks attributed to the hydroxyl OH. However, the addition of an inner-sphere water at neutral pH, as confirmed by large water shift and variable temperature ¹⁷O NMR experiments, is promising for water proton shift agents. The water proton shifts that are observed here for the Co(II) complexes are substantial, although not as large as we have observed for our best Co shift agents. ³²⁻³⁴ Co(II) complexes with four pendant hydroxyl groups on a 14-membered macrocycle produce water proton shifts that rival the best lanthanide(III) complexes.

The traditional agents for cellCEST contain Tm(III), Tb(III) or Dy(III) loaded into various mammalian cell lines. This study is the first report of cellCEST in a yeast system. The large proton shifts that we have observed for Co(II) complexes gives us confidence that transition metal cellCEST agents have promise. However, entrapment of the Co(II) complexes in organelles as well as the impervious nature of the yeast cell wall required high concentrations of Co(II) complex that are toxic to the yeast in order to observe a CEST effect. It is well established in the literature with Gd(III), that the cellular localization of the contrast agent is critical for optimum contrast due to differences in water exchange, and the method of uptake and localization may be important in the present study as well. However, a goal of future studies will be to develop Co(II) complexes of lowered toxicity to the yeast. Fluorophores with improved photophysical properties would be useful for studies of the uptake and compartmentalization of the complexes, although choice of fluorophore must be balanced with the need to maintain excellent solubility in water.

Acknowledgements

JRM thanks the NSF (CHE- 2004135) for support of this work. P.J.C is supported by a grant from the NIH (GM#098629). The authors would like to thank Chemistry Instrument Center (CIC), University at

Buffalo. This work utilized ICP-MS that was purchased with funding from a NSF Major Research Instrumentation Program (NSF CHE-0959565) and National Institutes of Health (S10 RR029517).

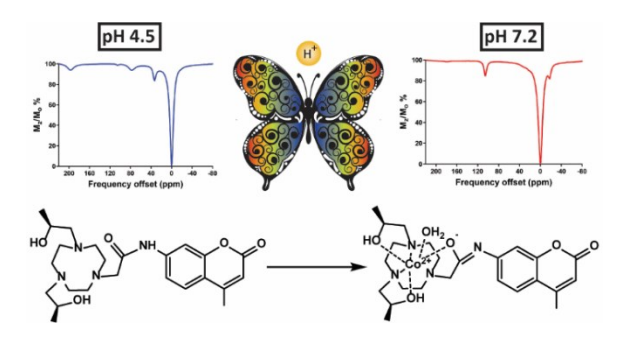
References

- 1. Zhang, S.; Merritt, M.; Woessner, D. E.; Lenkinski, R. E.; Sherry, A. D. PARACEST Agents: Modulating MRI Contrast via Water Proton Exchange. *Acc. Chem. Res.* **2003**, 36 (10), 783.
- 2. Zhang, S.; Malloy, C. R.; Sherry, A. D. MRI Thermometry Based on PARACEST Agents. *J. Am. Chem. Soc.* **2005**, 127 (50), 17572-17573.
- 3. van Zijl, P. C. M.; Yadav, N. N. Chemical exchange saturation transfer (CEST): What is in a name and what isn't? *Magn. Reson. Med.* **2011**, 65 (4), 927-948.
- 4. Vinogradov, E.; Sherry, A. D.; Lenkinski, R. E. CEST: From basic principles to applications, challenges and opportunities. *J. Magn. Reson.* **2013**, 229 (0), 155.
- 5. Ferrauto, G.; Delli Castelli, D.; Di Gregorio, E.; Terreno, E.; Aime, S. LipoCEST and cellCEST imaging agents: opportunities and challenges. *Nanomed.Nanobiotechol.* **2016**, 8 (4), 602-618.
- 6. Viswanathan, S.; Kovacs, Z.; Green, K. N.; Ratnakar, S. J.; Sherry, A. D. Alternatives to Gadolinium-Based Metal Chelates for Magnetic Resonance Imaging. *Chem. Rev.* **2010**, 110 (5), 2960-3018.
- 7. Zhang, S.; Malloy, Sherry, A. D. MRI thermometry based on PARACEST agents. *J. Am. Chem. Soc.* 2005, 127, 17572-17573.
- 8. Delli Castelli, D.; Terreno, E.; Aime, S. Yb(III)-HPDO3A: a dual pH- and temperature-responsive CEST agent. *Angew. Chem., Int. Ed.* **2011,** 50 (8), 1798-1800.
- 9. Dastrù, W.; Menchise, V.; Ferrauto, G.; Fabretto, S.; Carrera, C.; Terreno, E.; Aime, S.; Castelli, D. D. Modulation of the Prototropic Exchange Rate in pH-Responsive Yb-HPDO3A Derivatives as ParaCEST Agents. *Chem. Select* **2018**, 3 (22), 6035-6041.
- 10. Dorazio, S. J.; Tsitovich, P. B.; Gardina, S. A.; Morrow, J. R. The reactivity of macrocyclic Fe(II) paraCEST MRI contrast agents towards biologically relevant anions, cations, oxygen or peroxide. *J Inorg Biochem* **2012**, 117, 212-219.
- 11. Du, K; Waters, E. A.; Harris, T. D. Ratiometric quantitation of redox status with a molecular Fe₂ magnetic resonance probe. *Chem. Sci.* 2017, 8, 4424-4430.
- 12. Aime, S.; Delli Castelli, D.; Terreno, E. Supramolecular adducts between poly-L-arginine and [TmllIdotp]: A route to sensitivity-enhanced magnetic resonance imaging-chemical exchange saturation transfer agents. *Angew. Chem., Int. Ed.* **2003,** 42 (37), 4527.
- 13. Snoussi, K.; Bulte, J. W. M.; Guéron, M.; van Zijl, P. C. M. Sensitive CEST agents based on nucleic acid imino proton exchange: detection of poly(rU) and of a dendrimer-poly(rU) model for nucleic acid delivery and pharmacology. *Magn. Reson. Med.* **2003**, 49 (6), 998-1005.
- 14. Ali, M. M.; Yoo, B.; Pagel, M. D. Tracking the Relative In Vivo Pharmacokinetics of Nanoparticles with PARACEST MRI. *Mol. Pharmaceutics* **2009**, 6 (5), 1409-1416.
- 15. Khemtong, C.; Kessinger, C. W.; Gao, J. Polymeric nanomedicine for cancer MR imaging and drug delivery. *Chem. Commun.* **2009**, 24, 3497-3510.

- 16. Evbuomwan, O. M.; Terreno, E.; Aime, S.; Sherry, A. D. "CEST and PARACEST Agents for Molecular Imaging", in *The Chemistry of Molecular Imaging*. Long, N.; Wong, W.-T.; eds. 2014; Wiley & Sons, Hoboken, NJ: 2014, ch. 10 pp 225-243.
- 17. Ali, M. M.; Woods, M.; Suh, E. H.; Kovacs, Z.; Tircso, G.; Zhao, P.; Kodibagkar, V. D.; Sherry, A. D. Albumin-binding PARACEST agents. *J. Biol. Inorg. Chem.* **2007**, 12 (6), 855-865.
- 18. Aime, S.; Delli Castelli, D.; Terreno, E. Highly Sensitive MRI Chemical Exchange Saturation Transfer Agents Using Liposomes. *Angew. Chem., Int. Ed.* **2005**, 44 (34), 5513-5515.
- 19. Maruyama, S.; Ueda, J.; Kimura, A.; Murase, K. Development and Characterization of Novel LipoCEST Agents Based on Thermosensitive Liposomes. *Magn. Reson. Med. Sci.* **2016**, 15 (3), 324-334.
- 20. Opina, A. C. L.; Ghaghada, K. B.; Zhao, P.; Kiefer, G.; Annapragada, A.; Sherry, A. D. TmDOTA-Tetraglycinate Encapsulated Liposomes as pH-Sensitive LipoCEST Agents. *PLoS One* **2011**, 6 (11), e27370.
- 21. Ferrauto, G.; Di Gregorio, E.; Delli Castelli, D.; Aime, S. CEST-MRI studies of cells loaded with lanthanide shift reagents. *Magn. Reson. Med.* **2018**, 80 (4), 1626-1637.
- 22. Ferrauto, G.; Delli Castelli, D.; Di Gregorio, E.; Langereis, S.; Burdinski, D.; Grüll, H.; Terreno, E.; Aime, S. Lanthanide-Loaded Erythrocytes As Highly Sensitive Chemical Exchange Saturation Transfer MRI Contrast Agents. *J. Am. Chem. Soc.* **2014**, 136 (2), 638-641.
- 23. Nicholls, F. J.; Ling, W.; Ferrauto, G.; Aime, S.; Modo, M. Simultaneous MR imaging for tissue engineering in a rat model of stroke. *Sci. Rep.* **2015**, 5, 14597
- 24. Olatunde, A. O.; Cox, J. M.; Daddario, M. D.; Spernyak, J. A.; Benedict, J. B.; Morrow, J. R. Seven-Coordinate Coll, Fell and Six-Coordinate Nill Amide-Appended Macrocyclic Complexes as ParaCEST Agents in Biological Media. *Inorg. Chem.* **2014**, 53, 8311.
- 25. Tsitovich, P. B.; Cox, J. M.; Benedict, J. B.; Morrow, J. R. Six-coordinate Iron(II) and Cobalt(II) paraSHIFT Agents for Measuring Temperature by Magnetic Resonance Spectroscopy. *Inorg. Chem.* **2016**, 55 (2), 700.
- 26. Tsitovich, P. B.; Cox, J. M.; Spernyak, J. A.; Morrow, J. R. Gear up for a pH shift: a resonpsive iron(II) 2-amino-6-picolyl-appended macrocyclic paraCEST agent that protonates at a pendent group. *Inorg. Chem.* **2016**, 55, 12001.
- 27. Patel, A.; Asik, D.; Spernyak, J. A.; Cullen, P. J.; Morrow, J. R. MRI and fluorescence studies of Saccharomyces cerevisiae loaded with a bimodal Fe(III) T1 contrast agent. *J. Inorg. Biochem.* **2019,** 201, 110832.
- 28. Patel, A.; Asik, D.; Snyder, E. M.; Delillo, A. E.; Cullen, P. J.; Morrow, J. R. Binding and release of Fe(III) complexes from glucan particles for delivery of T1 MRI contrast agents. *ChemMedChem* 2020, 15, 1050-1057.
- 29. Tsitovich, P. B.; Spernyak, J. A.; Morrow, J. R. A redox-activated MRI contrast agent that switches between paramagnetic and diamagnetic states. *Angew. Chem., Int. Ed.* **2013,** 52 (52), 13997.
- 30. Wu, Y.; Zhou, Y.; Ouari, O.; Woods, M.; Zhao, P.; Soesbe, T. C.; Kiefer, G. E.; Sherry, A. D. Polymeric PARACEST Agents for Enhancing MRI Contrast Sensitivity. *J. Am. Chem. Soc.* **2008**, 130 (42), 13854-55.
- 31. Pikkemaat, J. A.; Wegh, R. T.; Lamerichs, R.; van de Molengraaf, R. A.; Langereis, S.; Burdinski, D.; Raymond, A. Y. F.; Janssen, H. M.; de Waal, B. F. M.; Willard, N. P.; Meijer, E. W.; Grüll, H. Dendritic PARACEST contrast agents for magnetic resonance imaging. *Contrast Media Mol. Imaging* **2007**, 2 (5), 229-239.
- 32. Abozeid, S. M.; Snyder, E. M.; Tittiris, T. Y.; Steuerwald, C. M.; Nazarenko, A. Y.; Morrow, J. R. Inner-Sphere and Outer-Sphere Water Interactions in Co(II) paraCEST Agents. *Inorg. Chem.* **2018**, 57 (4), 2085-2095.

- 33. Bond, C. J.; Sokolow, G. E.; Crawley, M. R.; Burns, P. J.; Cox, J. M.; Mayilmurugan, R.; Morrow, J. R. Exploring Inner-Sphere Water Interactions of Fe(II) and Co(II) Complexes of 12-Membered Macrocycles To Develop CEST MRI Probes. *Inorg. Chem.* **2019**, 58 (13), 8710-8719.
- 34. Abozeid, S. M.; Asic, D.; Sokolow, G. E.; Lovell, J.; Nazarenko, A.; Morrow, J. R. Co(II) Complexes as Liposomal CEST Agents. *Angew. Chem. Int. Ed.* 2020, 59, 12093-12097.
- 35. Piguet, C. Paramagnetic Susceptibility by NMR: The "Solvent Correction" Removed for Large Paramagnetic Molecules. *J. Chem. Educ.* **1997,** 74 (7), 815-816..
- 36. Evans, D. F. 400. The determination of the paramagnetic susceptibility of substances in solution by nuclear magnetic resonance. *J. Chem. Soc.* **1959**, (0), 2003-2005.
- 37. Bain, G. A.; Berry, J. F. Diamagnetic Corrections and Pascal's Constants. *Journal of Chemical Education* **2008**, 85 (4), 532-33.
- 38. Soesbe, T. C.; Togao, O.; Takahashi, M.; Sherry, A. D. SWIFT-CEST: a new MRI method to overcome T(2) shortening caused by PARACEST contrast agents. *Magn Reson Med* **2012**, 68 (3), 816-21.
- 39. Gimeno, C. J. L., P. O.; Styles, C. A.; Fink, G. R., . Unipolar cell divisions in the yeast S. cerevisiae lead to filamentous growth: regulation by starvation and RAS. *Cell* **1992**, 68 (6), 1077-90.
- 40. Cullen, P. J.; Sabbagh, W., Jr.; Graham, E.; Irick, M. M.; van Olden, E. K.; Neal, C.; Delrow, J.; Bardwell, L.; Sprague, G. F., Jr. A signaling mucin at the head of the Cdc42- and MAPK-dependent filamentous growth pathway in yeast. *Genes Dev* **2004**, 18 (14), 1695-708.
- 41. Kovacs, D.; Kiraev, S. R.; Phipps, D.; Orthaber, A.; Borbas, K. E. Eu(III) and Tb(III) Complexes of Octa- and Nonadentate Macrocyclic Ligands Carrying Azide, Alkyne, and Ester Reactive Groups. *Inorg. Chem.* **2020**, 59 (1), 106-117.
- 42. Kovacs, D.; Lu, X.; Mészáros, L. S.; Ott, M.; Andres, J.; Borbas, K. E. Photophysics of Coumarin and Carbostyril-Sensitized Luminescent Lanthanide Complexes: Implications for Complex Design in Multiplex Detection. *J. Am. Chem. Soc.* **2017**, 139 (16), 5756-5767.
- 43. Gandioso, A.; Bresolí-Obach, R.; Nin-Hill, A.; Bosch, M.; Palau, M.; Galindo, A.; Contreras, S.; Rovira, A.; Rovira, C.; Nonell, S.; Marchán, V. Redesigning the Coumarin Scaffold into Small Bright Fluorophores with Far-Red to Near-Infrared Emission and Large Stokes Shifts Useful for Cell Imaging. *J. Org. Chem.* **2018**, 83 (3), 1185-1195.
- 44. Didar Asik, R. S., Samira M. Abozeid, Travis B. Mitchell, Steven G. Turowski, Joseph A. Spernyak and Janet R. Morrow. Modulating the Properties of Fe(III) Macrocyclic MRI Contrast Agents by Appending Sulfonate or Hydroxyl Groups. *Molecules* **2020**, 25 (10), 2291.
- 45. Dorazio, S. J.; Olatunde, A. O.; Spernyak, J. A.; Morrow, J. R. CoCEST: cobalt(ii) amide-appended paraCEST MRI contrast agents. *Chem. Commun.* **2013**, 49 (85), 10025-10027.
- 46. Maigut, J.; Meier, R.; Zahl, A.; Eldik, R. v. Triggering Water Exchange Mechanisms via Chelate Architecture. Shielding of Transition Metal Centers by Aminopolycarboxylate Spectator Ligands. *J. Am. Chem. Soc.* **2008**, 130 (44), 14556.
- 47. Gale, E. M.; Zhu, J.; Caravan, P. Direct Measurement of the Mn(II) Hydration State in Metal Complexes and Metalloproteins through 170 NMR Line Widths. *J. Am. Chem. Soc.* **2013**, 135 (49), 18600-18608..
- 48. Tsitovich, P. B.; Morrow, J. R. Macrocyclic ligands for Fe(II) paraCEST and chemical shift MRI contrast agents. *Inorg. Chim. Acta* **2012**, 393, 3-11.
- 49. Kawai, S.; Hashimoto, W.; Murata, K. Transformation of Saccharomyces cerevisiae and other fungi. *Bioengineered Bugs* **2010**, 1 (6), 395-403.
- 50. Smith, P. K.; Krohn, R. I.; Hermanson, G. T.; Mallia, A. K.; Gartner, F. H.; Provenzano, M. D.; Fujimoto, E. K.; Goeke, N. M.; Olson, B. J.; Klenk, D. C. Measurement of protein using bicinchoninic acid. *Anal. Biochem.* **1985**, 150 (1), 76-85.

- 51. Yu, M.; Bouley, B. S.; Xie, D.; Enriquez, J. S.; Que, E. L. 19F PARASHIFT Probes for Magnetic Resonance Detection of H2O2 and Peroxidase Activity. *J. Am. Chem. Soc.* **2018**, 140 (33), 10546-10552 DOI: 10.1021/jacs.8b05685.
- 52. Xie, D.; Yu, M.; Kadakia, R. T.; Que, E. L. 19F Magnetic Resonance Activity-Based Sensing Using Paramagnetic Metals. *Acc. Chem. Res.* **2020**, 53 (1), 2-10.
- 53. Mulas, G.; Ferrauto, G.; Dastrù, W.; Anedda, R.; Aime, S.; Terreno, E. Insights on the relaxation of liposomes encapsulating paramagnetic Ln-based complexes. *Magn. Reson. Med.* **2015**, 74 (2), 468-473.
- 54. Castelli, D. D.; Terreno, E.; Longo, D.; Aime, S. Nanoparticle-based chemical exchange saturation transfer (CEST) agents. *NMR Biomed.* **2013**, 26 (7), 839-849.
- 55. Ferrauto, G.; Di Gregorio, E.; Dastrù, W.; Lanzardo, S.; Aime, S. Gd-loaded-RBCs for the assessment of tumor vascular volume by contrast-enhanced-MRI. *Biomaterials* **2015**, 58, 82-92.
- 56. Cullen, P. J.; Sprague, G. F. The Regulation of Filamentous Growth in Yeast. *Genetics* **2012**, 190 (1), 23-49.
- 57. Karunanithi, S.; Cullen, P. J. The Filamentous Growth MAPK Pathway Responds to Glucose Starvation Through the Mig1/2 Transcriptional Repressors in Saccharomyces cerevisiae" *Genetics* **2012**, 192 (3), 869-887.
- 58. Adhikari, H.; Vadaie, N.; Chow, J.; Caccamise, L. M.; Chavel, C. A.; Li, B.; Bowitch, A.; Stefan, C. J.; Cullen, P. J. Role of the Unfolded Protein Response in Regulating the Mucin-Dependent Filamentous-Growth Mitogen-Activated Protein Kinase Pathway. *Mol. Cell. Biol.* **2015**, 35 (8), 1414-1432..
- 59. González, B.; Mas, A.; Beltran, G.; Cullen, P. J.; Torija, M. J. Role of Mitochondrial Retrograde Pathway in Regulating Ethanol-Inducible Filamentous Growth in Yeast. *Front. Physiol.* **2017**, 8, 148.
- 60. Nass, R.; Rao, R. The yeast endosomal Na+/H+ exchanger, Nhx1, confers osmotolerance following acute hypertonic shock. *Microbiology* **1999**, 145 (11), 3221-3228.
- 61. Trollmo, C.; André, L.; Blomberg, A.; Adler, L. Physiological overlap between osmotolerance and thermotolerance in Saccharomyces cerevisiae. *FEMS Microbiol. Lett.* **1988**, 56 (3), 321-325.
- 62. Daniel Gietz, R.; Woods, R. A. In *Methods in Enzymology*; Guthrie, C., Fink, G. R., Ed.; Academic Press: 2002; Vol. 350, pp 87-96.
- 63. Terreno, E.; Geninatti Crich, S.; Belfiore, S.; Biancone, L.; Cabella, C.; Esposito, G.; Manazza, A. D.; Aime, S. Effect of the intracellular localization of a Gd-based imaging probe on the relaxation enhancement of water protons. *Magn. Reson. Med.* **2006**, 55 (3), 491-497..



High spin Co(II) complexes with an appended fluorophores show a large pH-dependent shift in CEST (chemical exchange saturation transfer) peak position and in water proton shifts as pH responsive agents. These bimodal agents associate with yeast (*S. cerevisiae*) to produce the first examples of transition metal based cellCEST.